Available online www.ejaet.com

European Journal of Advances in Engineering and Technology, 2018, 5(2): 106-112

Research Article ISSN: 2394 - 658X

Mechanical Properties and Microstructure Evaluation of Biomaterial Grade 316L Stainless Steel Produced by Additive Manufacturing

KV Sudhakar, Penn Rawn, Ronda Coguill, Scott Coguill, Taylor Winsor and Bruce Madigan

Montana Tech of the University of Montana, Butte, MT 59701, USA
kvsudhakar@mtech.edu

ABSTRACT

In this investigation, 316L stainless steel, one of the three metal alloy grades used as a biomaterial, is produced by a selective laser melting process (SLM) of additive manufacturing. Static properties and microstructures including fracture morphologies were investigated as a function of build angles of 0, 30, 60, and 90 degrees. Static properties, namely elastic modulus, yield strength, ultimate tensile strength, and percent elongation were evaluated using a MTS landmark servo hydraulic machine. Microstructures were characterized using a Leica DM750P optical microscope, paired with Leica application suite software. Tensile fracture surfaces were investigated with LEO-VP SEM instrument. The SLM processed 316L biomaterial grade stainless steel showed tensile properties of elastic modulus and ultimate tensile strength similar to wrought material, while exhibiting differences for the yield and % elongation properties. Microstructures demonstrated a heterogeneous structure with melt pool boundaries, columnar and cellular dendrites with pores and voids. The fracture morphologies showed ductile mode of fracture demonstrating a good level of strength and ductility required as a synthetic biomaterial.

Keywords*:* 316L biomaterial grade stainless steel, additive manufacturing, static properties, microstructure, tensile fracture morphologies

INTRODUCTION

Additive manufacturing or 3D-printing process involving selective laser melting (SLM) is an innovative manufacturing technique to produce components in layer-by-layer manner to a near/net shaped products [1]. SLM is a manufacturing process dictated by input parameters that result in various non-equilibrium physical phenomena [2]. It is used to produce complex parts which cannot be manufactured using conventional processes such as casting or forging. The final quality of the produced component is dependent on various factors like microstructure, mechanical properties, pores, voids, and the residual stresses [2-4]. 316L SS is well-known for its applications as a biomaterial for manufacturing a number of medical devices [5-7]. One of the challenges with SLM processing of 316L SS is to minimize (if not avoid completely) residual porosity and poor surface quality. These requirements are critical, especially for biomedical applications requiring high static and dynamic properties, ductility, and high corrosion resistance. Because of this, the major focus of research is to evaluate the effect of SLM processing parameters on mechanical property, microstructure and fracture [8-10]. Various selective laser melting processing parameters have been investigated to get full density parts [11-13]. Many investigators [14-18] have revealed that the SLM processing parameters do influence the porosity, mechanical properties and quality of SS.

SLM biomaterial implants needs to have the same Young's modulus as current SS implants. There is a need to examine the SLM produced 316 L parts for biomedical applications. In this regard it is important to evaluate the mechanical properties, microstructure, and fracture morphologies of SLM parts to replace conventionally produced (wrought) 316L parts. The objective of the present work is to evaluate the effect of specimen build angle orientation on the SLM processing, mechanical properties, microstructure, and fracture morphologies of 316L stainless steel used as a biomaterial.

MATERIALS AND METHODS

Material/Alloy

The chemical composition of the 316 L stainless steel used in the present investigation is detailed in Table 1 and the powder particles of 316L SS are shown in Figure 1.

Table -1 Chemical Composition of Stainless Steel (AISI 316L)

Element	C	Cr	Ni	Mo	Co	Si
Wt.%	0.02	16.9	12.1	2.4	0.06	0.5

Selective Laser Melting (SLM) Process Parameters

SLM process parameters used in this investigation are outlined in Table -2.

Table -2 SLM Process Parameters Used

Process Parameters	Details/measurements
Hatch spacing	0.09 mm
Stripe width	5.00 mm
Layer thickness	0.02 mm
Speed	1083 mm/s
Beam offset	0.003 mm
Stripes overlap	0.12 mm
Power	195 W
Global energy density	$2.0\frac{J}{mm^2}$ or $100\frac{J}{mm^3}$

Static Testing

The tensile testing for all of the 316L stainless steel specimens were carried out on a MTS Landmark servo hydraulic Test System as per the ASTM E8/E8M standard. The diameter of the reduced section was 8.96 mm and the gage length was 35.6 mm. Figure 2 shows the tensile test specimen.

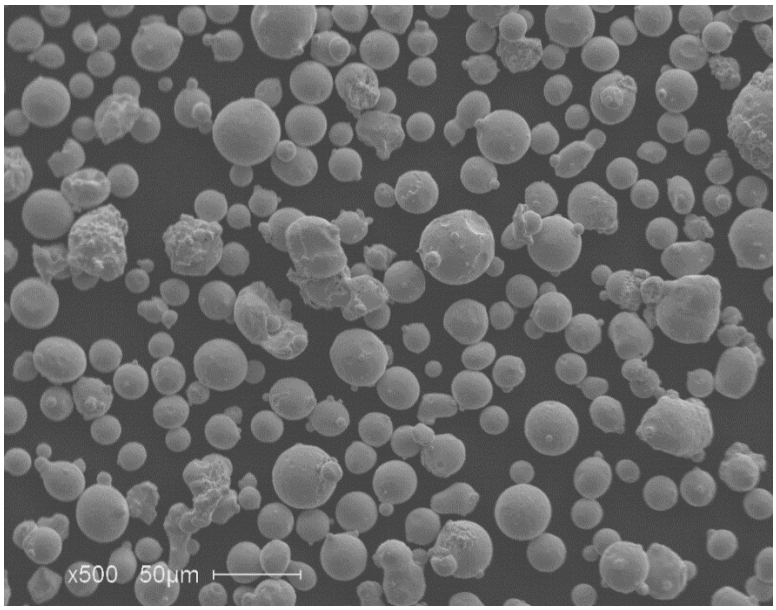

Fig. 1 316L Stainless steel powder particles

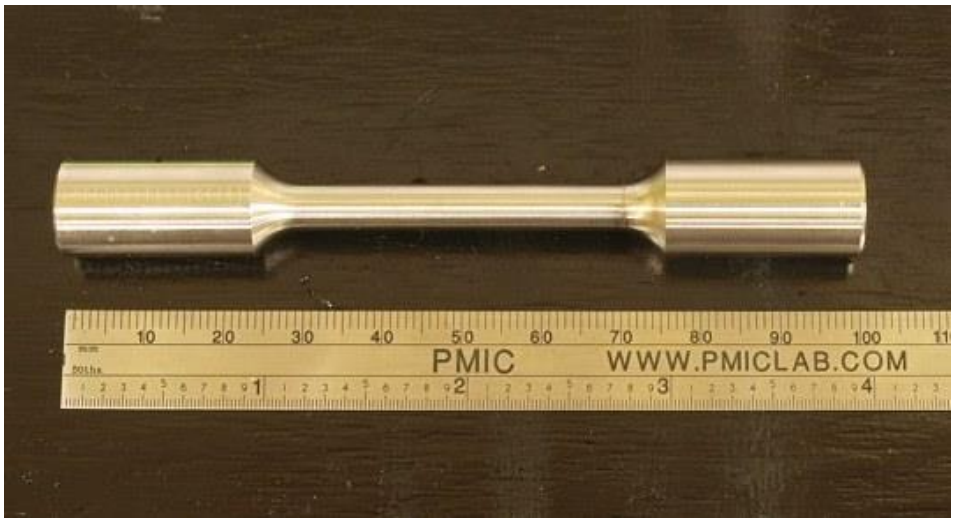

Fig. 2 316L Stainless Steel Tensile Test Specimen

RESULTS AND DISCUSSION

Evaluation of Static Properties

The elastic modulus and yield strength of 316L SS with respect to specimen build orientations are presented in Figure 3 and Figure 4, respectively. Elastic modulus of SLM specimens was determined to be on par with the wrought specimens tested as shown in Figure 3. As can be seen from Figure 4 that yield strength of SLM samples were 20 to 30% higher in comparison to that of wrought samples. The very fine microstructures of SLM stainless steel is typically responsible for an increase in yield strength as discussed further on in microstructure characterization section. Among the SLM samples, 90-degree specimen orientation showed, relatively, a lower value of yield strength. This is primarily attributed to the loading angle of the test specimen being at right angles to the solidified melt pool build plane.

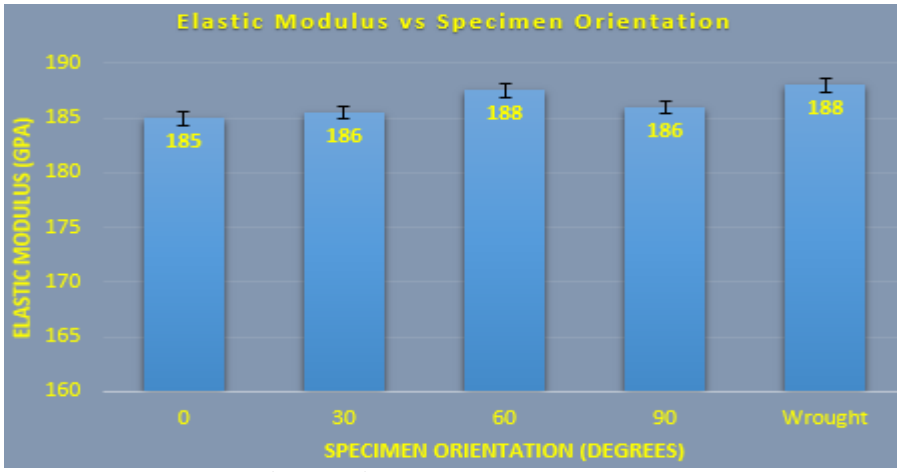

Fig. 3 Elastic Modulus as a function of Specimen Orientation (bars represent build orientation)

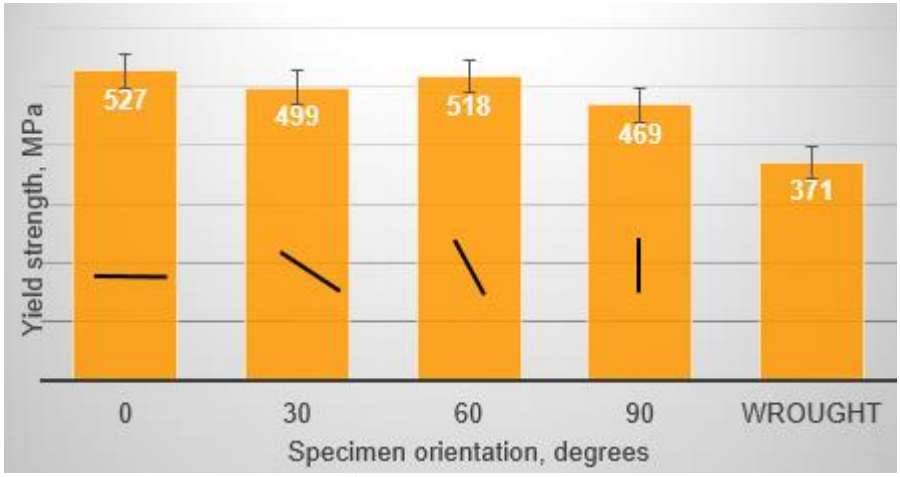

Fig. 4 Yield strength as a function of Specimen Orientation (bars represent build orientation)

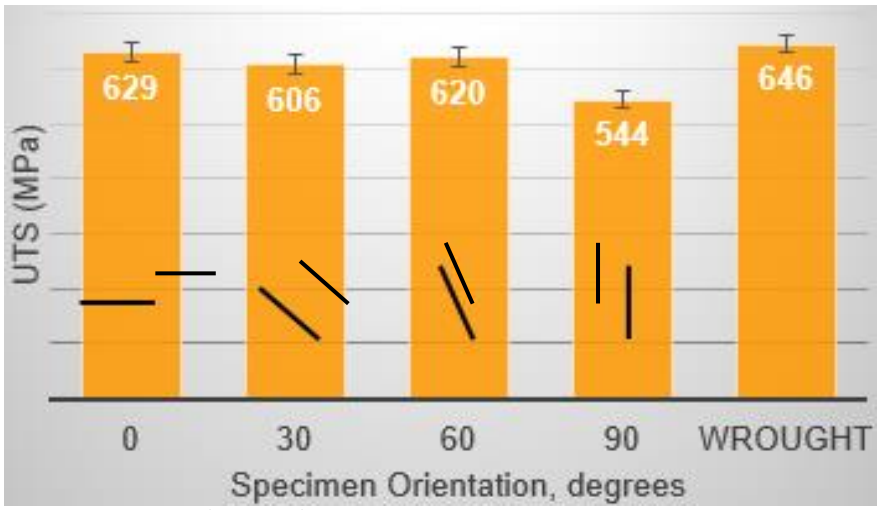

Fig. 5 UTS as a function of Specimen Orientation (bars represent build orientation)

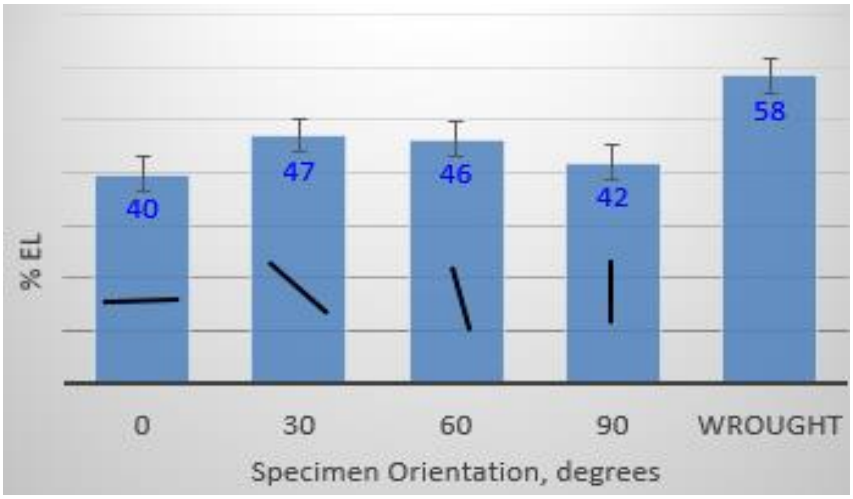

Fig. 6 Percent elongation vs. specimen orientation (bars represent build orientation)

Ultimate tensile strength and percent elongation of 316L with respect to specimen orientations are summarized in Figure 5 and Figure 6, respectively. It is demonstrated in Figure 5 that the UTS values for SLM specimens and the wrought samples were almost on par with each other with the exception of the 90 º specimens. Percent elongation of wrought samples were 19 to 29% higher in comparison to that of SLM samples, as shown in Figure 6. The lower values of elongation in SLM SS samples is attributed to the finer heterogeneous microstructure consisting of melt pool boundaries, porosity and voids.

Microstructure Characterization

Microstructures of 316L were investigated and were etched using the etchants; Kalling's reagent (5 g $CuCl_2$, 100 ml HCl, and 100 ml Ethanol) and Villella's reagent (1 g Picric acid, 5 ml HCl, 100 ml Ethanol). Microstructures of wrought SS samples are shown in Figure 7 and 8 that consist of predominantly carbide precipitates in SS matrix. The carbide precipitates are formed due to the strong affinity of alloying elements Cr, Ni, Mo with carbon.

SLM samples' microstructures are revealed in Figures 9 and 10. They are characterized by the presence of melt pool structures with pores and voids. The characteristic cellular structure is formed as a result of high rate of melting and cooling of melted stainless steel powders in thin layers. The concentric lines, as shown in Figure 10, are formed because of the solidification front that moves forward in the form of waves as opposed to a constant pattern due to the solidification enthalpy [19]. Epitaxial phase growth is known to contribute to better mechanical properties and the epitaxial laser melting process depends on thermal gradient and growth speed [20]. During laser melting process, higher thermal gradients induce columnar instead of equiaxed grain growth [21]. As can be clearly seen, the microstructures of additively manufactured stainless steel are distinctly different in comparison to wrought stainless steel.

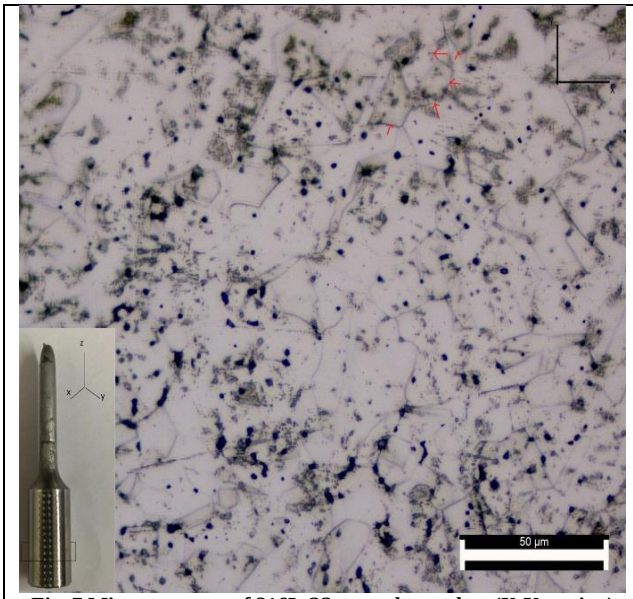

Fig. 7 Microstructure of 316L SS wrought test bar (X-Y section) demonstrating the presence of randomly oriented equiaxed grains with carbide precipitates. Etched with Kalling's Reagent

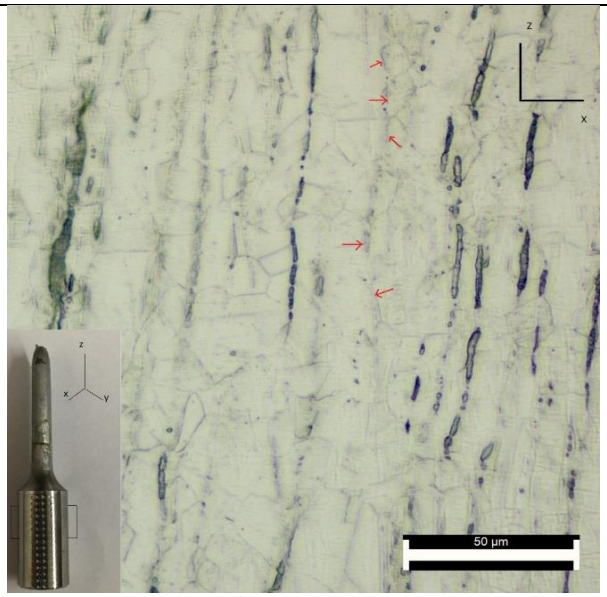

Fig. 8 Microstructure of 316L SS wrought test bar (Z-section) demonstrating the presence of randomly oriented equiaxed grains with carbide precipitates. Etched with Kalling's Reagent

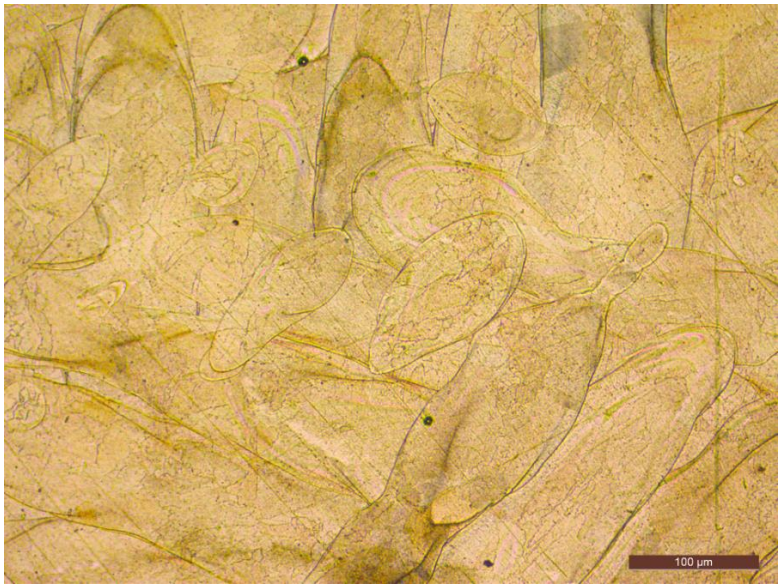

Fig. 9 3D Printed 316L SS: Demonstration of the presence of melt pool boundaries. Etched with Kalling's Reagent

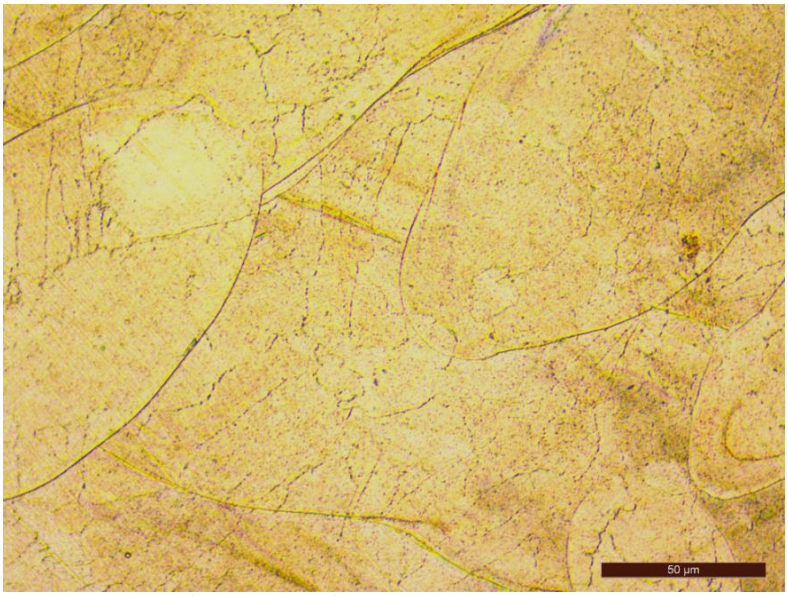

Fig. 10 3D Printed 316L SS: Demonstration of the presence of cellular structure inside melt pool network Etched with Kalling's Reagent

Investigation of Fractographic Modes

The titanium samples were examined using a LEO 1430VP scanning electron microscope.

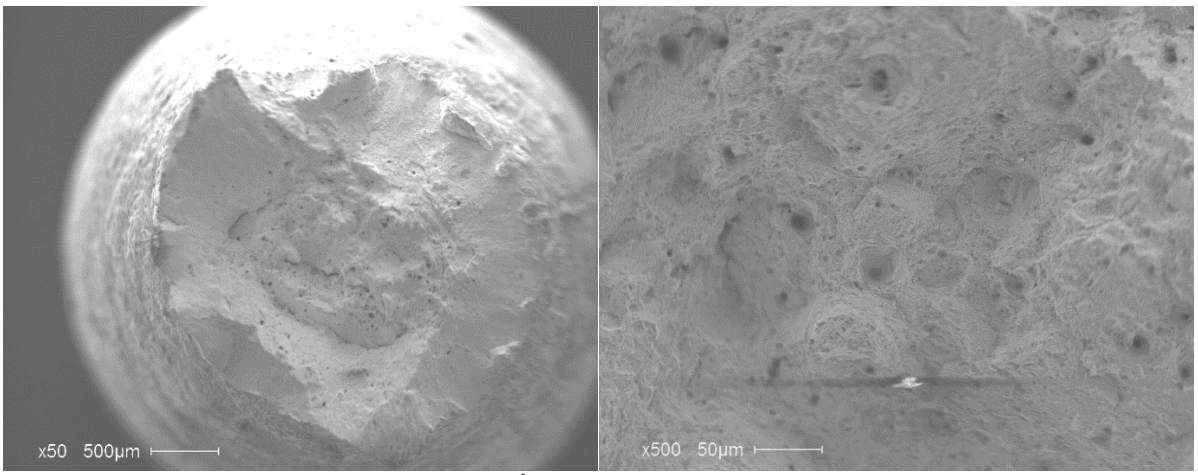

Fig. 11 Tensile test specimen with 0^0 build orientation revealing ductile fracture features

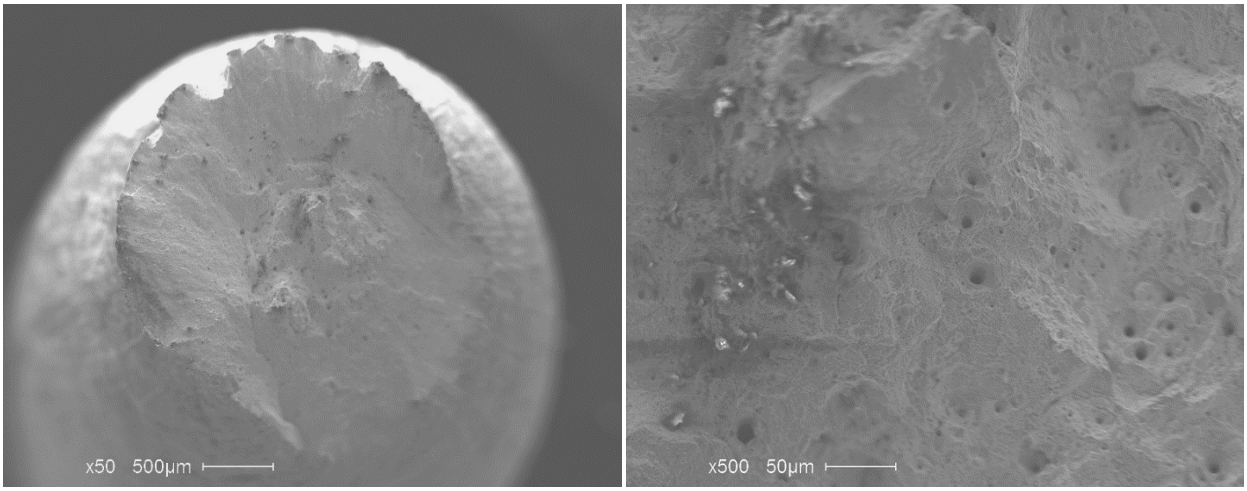

Fig. 12 Tensile test specimen with 60^0 build orientation revealing ductile fracture features

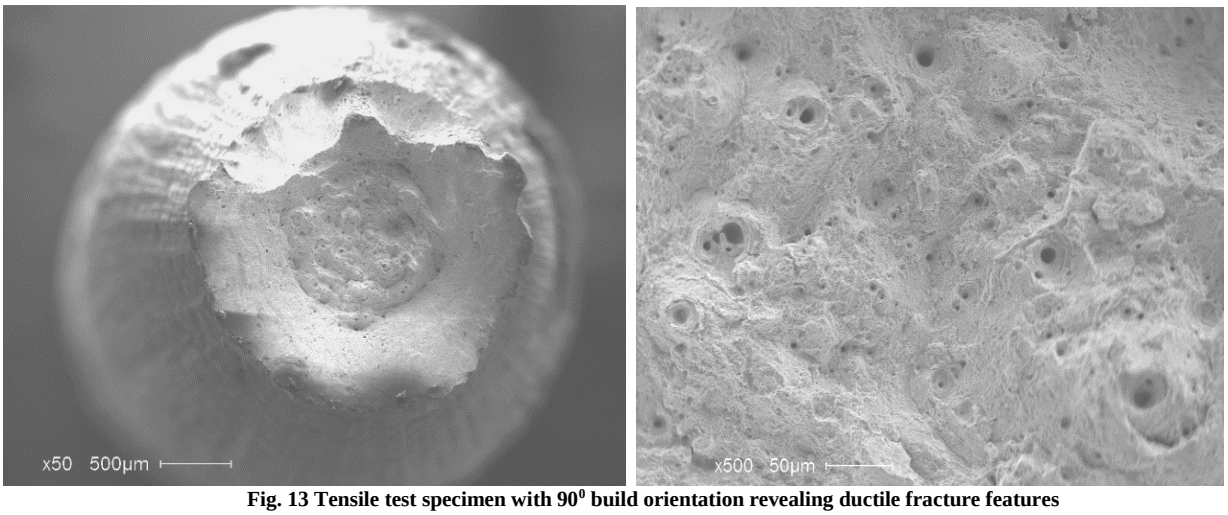

Fig. 13 Tensile test specimen with 90^0 build orientation revealing ductile fracture features

The fractographic features in Figure 11 through 13 clearly demonstrate ductile mode of fracture characterized by the presence of voids, dimples, and ductile ridges. These ductile features contributed similar mechanical properties for the 0º, 30º, and 60º build orientation specimens. The 90º specimens exhibited a marginal difference in mechanical properties.

CONCLUSION

The experimental result shows that applying the template of half eye gives a satisfying result in the frontal face image. Furthermore, applying composite template produces better results of eye detection through all orientations. In order to detect head poses in the face image, three templates were generated to represent the entire face; in frontal case and both profile cases. Finally, a detection rate of 98.83% was reported by applying the proposed method on PICS Database while it is 93.87% for the templates which have entire eye image.

- SLM printed 316L SS biomaterial grade samples demonstrated tensile properties of elastic modulus and ultimate tensile strength similar to wrought material, while exhibiting differences for the yield and % elongation properties.
- Zero-degree build angle provided relatively higher yield and ultimate tensile strengths in comparison to 30, 60, and 90-degree build angle orientations of the specimen.
- SLM 316L SS biomaterial grade samples demonstrated a non-equilibrium heterogeneous microstructure with voids, pores and melt pool networks with cellular structure.
- Microstructures of SLM samples showed overlapped, segregated melt pools with distinct boundaries that are similar to weld fillets.
- Both printed and wrought 316L SS tensile samples exhibited predominantly ductile fracture features characterized by dimples, voids and ductile ridges.

Acknowledgement

"Research was sponsored by the Army Research Laboratory and was accomplished under Cooperative Agreement Number W911NF-15-2-0020. The views and conclusions contained in this document are those of the authors and should not be interpreted as representing the official policies, either expressed or implied, of the Army Research Laboratory or the U.S. Government. The U.S. Government is authorized to reproduce and distribute reprints for Government purposes notwithstanding any copyright notation herein."

The authors wish to thank Mr. Gary Wyss, Senior Scientist, CAMP, for SEM data analysis.

REFERENCES

[1] JA Cherry, HM Davies, S Mehmood, NP Lavery, SGR Brown and J Sienz, Investigation into the Effect of Process Parameters on Microstructural and Physical Properties of 316L Stainless Steel Parts by Selective Laser Melting, *International Journal of Advanced Manufacturing Technology*, **2015**, 76, 869–879.
[2] M Averyanova, E Cicala, P Bertrand and D Grevey, Experimental Design Approach to Optimize Selective Laser Melting of Martensitic 17-4 PH Powder: Part I – Single Laser Tracks and First Layer, *Rapid Prototyping Journal*, **2012**, 18, 28–37.
[3] MH Farshidianfar, *Control of Microstructure in Laser Additive Manufacturing*, M.Sc. Thesis, University of Waterloo, Canada, **2014**, 1-123.
[4] JP Kruth, M Badrossamay, E Yasa, J Deckers, L Thijs and J Van Humbeeck, Part and Material Properties in Selective Laser Melting of Metals, *16th International Symposium on Electromachining* (ISEM XVI), **2010**, 1-12.
[5] A Gebhardt, FM Schmidt, JS Hötter, W Sokalla and P Sokalla, Additive Manufacturing by Selective Laser Melting the Realizer Desktop Machine and its Application for the Dental Industry, *Physics Procedia*, **2010**, 5, 543–549.
[6] L Hao, S Dadbakhsh, O Seaman and M Felstead, Selective Laser Melting of a Stainless Steel and Hydroxyapatite Composite for Load-Bearing Implant Development, *Journal of Materials Processing Technology*, **2009**, 209, 5793–5801.
[7] X Su, Y Yang, Research on Track Overlapping During Selective Laser Melting of Powders, *Journal of Materials Processing Technology*, **2012**, 212, 2074–2079.
[8] AN Chatterjee, S Kumar, P Saha, PK Mishra and AR Choudhury, An Experimental Design Approach to Selective Laser Sintering of Low Carbon Steel, *Journal of Materials Processing Technology*, **2003**, 136, 151–157.
[9] JP Kruth, L Froyen, JV Vaerenbergh, P Mercelis, M Rombouts and B Lauwers, Selective Laser Melting of Iron-Based Powders, *Journal of Materials Processing Technology*, **2004**, 149, 616–622.
[10] JP Kruth, P Mercelis, J Van Vaerenbergh, L Froyen and M Rombouts, Binding Mechanisms in Selective Laser Sintering and Selective Laser Melting, *Rapid Prototype Journal*, **2005**, 11, 26–36.
[11] S Dadbakhsh, L Hao and N Sewell, Effect of Selective Laser Melting Layout on the Quality of Stainless Steel Parts, *Rapid Prototyping Journal*, **2012**, 18, 241–249.
[12] R Li, Y Shi, Z Wang, L Wang, J Liu and W Jiang, Densification Behavior of Gas and Water Atomized 316l Stainless Steel Powder During Selective Laser Melting, *Applied Surface Science*, **2010**, 256, 4350–4356.
[13] M Rombouts, JP Kruth, L Froyen and P Mercelis, Fundamentals of Selective Laser Melting of Alloyed Steel Powders, *CIRP Annual Manufacturing Technology*, **2006**, 55, 187–192.
[14] MSF de Lima and S Sankaré, Microstructure and Mechanical Behavior of Laser Additive Manufactured AISI 316 Stainless Steel Stringers, *Materials Design*, **2014**, 55, 526–532.
[15] I Tolosa, F Garciandia, F Zubiri, F Zapirain, A Esnaola, Study of Mechanical Properties of AISI 316 Stainless Steel Processed by 'Selective Laser Melting', Following Different Manufacturing Strategies, *International Journal of Advanced Manufacturing Technology*, **2010**, 51, 639–647.
[16] B Zhang, L Dembinski and C Coddet, The Study of the Laser Parameters and Environment Variables Effect on Mechanical Properties of High Compact Parts Elaborated by Selective Laser Melting 316L Powder, *Materials Science and Engineering A*, **2013**, 584, 21–31.
[17] B Verlee, T Dormal and J Lecomte-Beckers, Density and Porosity Control of Sintered 316L Stainless Steel Parts Produced by Additive Manufacturing, *Powder Metallurgy*, **2012**, 55, 260–267.
[18] L Wang, P Pratt, SD Felicelli, H El Kadiri, JT Berry, PT Wang and MF Horstemeyer, TMS, Experimental Analysis of Porosity Formation in Laser-Assisted Powder Deposition Process, *Minerals, Metals & Materials Society*, Warrendale, **2009**, 1-23.
[19] GM Oreper and J Szekely, Heat and Fluid-Flow Phenomena in Weld Pools, *Journal of Fluid Mechanics*, **1984**, 147, 53–79.
[20] M Gaumann, S Henry, F Cleton, JD Wagniere, W Kurz, Epitaxial Laser Metal Forming: Analysis of Microstructure Formation, *Materials Science and Engineering A*, 1**999**, 271, 232-241.
[21] Milton Sergio Fernandes de Lima and Simon Sankare, Microstructure and Mechanical Behavior of Laser Additive Manufactured AISI 316 Stainless Steel Stringers, *Materials and Design*, **2014**, 55, 526-532.